

Lead Halide Perovskite Nanostructures for Dynamic Color Display

Yisheng Gao,^{†,#} Can Huang,^{†,#} Chenglong Hao,[‡] Shang Sun,[†] Lei Zhang,[‡] Chen Zhang,[†] Zonghui Duan,[†] Kaiyang Wang,[†] Zhongwei Jin,[‡] Nan Zhang,[†] Alexander V. Kildishev,[§] Cheng-Wei Qiu,^{*,‡,||} Qinghai Song,^{*,†,⊥} and Shumin Xiao^{*,†,⊥}

[†]State Key Laboratory on Tunable Laser Technology, Ministry of Industry and Information Technology Key Lab of Micro-Nano Optoelectronic Information System, Shenzhen Graduate School, Harbin Institute of Technology, Shenzhen 518055, China

[‡]Department of Electrical and Computer Engineering, National University of Singapore, 4 Engineering Drive 3, Singapore 117583, Singapore

[§]School of Electrical and Computer Engineering and Birck Nanotechnology Center, Purdue University, West Lafayette, Indiana 47907, United States

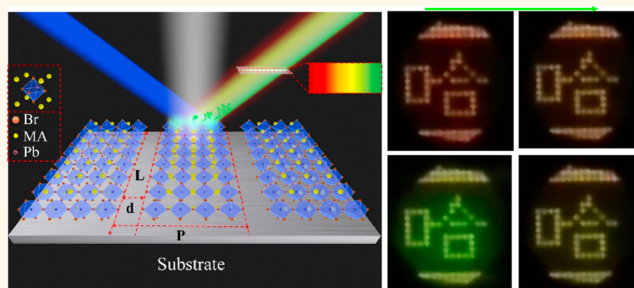
^{||}SZU-NUS Collaborative Innovation Center for Optoelectronic Science and Technology, Shenzhen University, Shenzhen 518060, China

[⊥]Collaborative Innovation Center of Extreme Optics, Shanxi University, Taiyuan 030006, China

Supporting Information

ABSTRACT: Nanoprint-based color display using either extrinsic structural colors or intrinsic emission colors is a rapidly emerging research field for high-density information storage. Nevertheless, advanced applications, e.g., dynamic full-color display and secure information encryption, call for demanding requirements on *in situ* color change, nonvacuum operation, prompt response, and favorable reusability. By transplanting the concept of electrical/chemical doping in the semiconductor industry, we demonstrate an *in situ* reversible color nanoprinting paradigm via photon doping, triggered by the interplay of structural colors and photon emission of lead halide perovskite gratings. It solves the aforementioned challenges at one go. By controlling the pumping light, the synergy between interlaced mechanisms enables color tuning over a large range with a transition time on the nanosecond scale in a nonvacuum environment. Our design presents a promising realization of *in situ* dynamic color nanoprinting and will empower the advances in structural color and classified nanoprinting.

KEYWORDS: color printing, structural color, dynamic color, lead halide perovskite, nanostructures



Various colors of living creatures are one of the most precious gifts offered by nature. The vivid colors have enriched humans' life and also aroused curiosity in chasing the secrets behind them. It turns out that many vibrant colors originate from the interaction between visible light and the "structures" of creatures.^{1–7} Inspired by this effect, nanostructure-based light–matter interaction has emerged to produce vivid and vibrant colors, which relies on controlling the geometric parameters of nanostructures, termed extrinsic structural color.^{8–10} Among the reported structural colors, plasmonic color printing outperforms traditional pigment- or dye-based color printing in their ultrahigh subwavelength resolution, huge optical data storage, and ultracompact size.^{11–17} Generally, the inherent absorption of materials used in the visible range usually gives broad and less intensive resonance, which significantly degrades the brightness and

contrast of generated colors, although highly absorbing films of a few to tens of nanometers in thickness on a metal film can support decent colors based on selective absorption of visible light.¹⁸ In order to improve the color impression, high-index dielectric materials with low losses in the visible range have been explored. By using all-dielectric materials, color contrast can be improved over the whole visible spectrum.^{19–24} However, most color nanoprintings work in a static way, which limits their advanced applications, such as anticounterfeiting, dynamic full-color display, and highly secure encryption. In analogy to electrical doping and chemical doping, which have been widely used in the mature semiconductor industry

Received: March 31, 2018

Accepted: July 31, 2018

Published: August 16, 2018

for control over the electrical and optical properties of semiconductors, recently, the concept of doping has been successfully transplanted to control color nanoprintings in a dynamic way, such as by infiltrating liquid crystals into plasmonic nanostructures or controlling the hydrogenation/dehydrogenation kinetics of metal nanoparticles.^{25–31} However, none of them can realize an *in situ* control, and a hydrogen/oxygen environment is even required in the latter method.

In addition to extrinsic structural color, photoluminescence (PL) from active materials, termed intrinsic emission color, can also be used for color display, *e.g.*, microsized light-emitting devices (LEDs) and laser diode based color displays.^{32–37} Lately, methylammonium lead halide perovskite (MAPbX₃, where MA = CH₃NH₃⁺ and X = Cl, Br, I, or their mixture), one type of semiconductors, has drawn a lot of attention due to its excellent PL properties, such as high quantum efficiency and narrow full-width at half-maximum (fwhm).^{32–35,38–40} However, MAPbX₃-based color displays are usually static and low-resolution. Although the emission peaks can be postsynthetically tuned with anion exchange,^{35,41,42} the color variation time is too long and cannot be controlled *in situ*, not to mention extreme requirements on ambient conditions.

RESULTS AND DISCUSSION

Working Principle of the Reversible Color Display.

In this work, in analogy to electrical/chemical doping, we propose an *in situ* reversible color nanoprinting paradigm *via* photonic doping, triggered by the interplay of structural colors and photon emission of MAPbX₃ gratings. The working principle is illustrated in Figure 1, where both white light and laser light

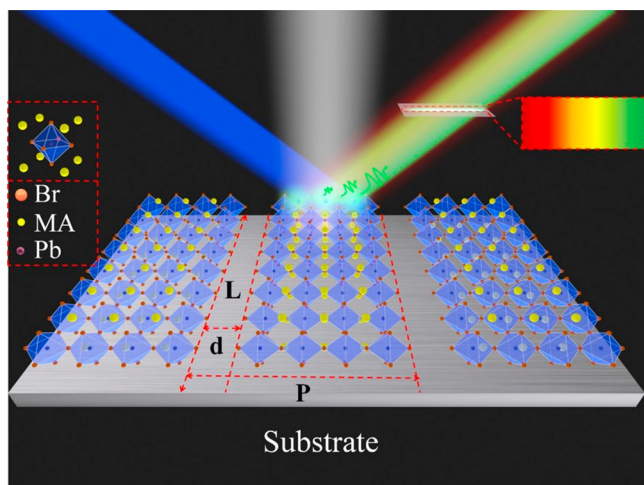


Figure 1. Working principle. The schematic design of pixels and the *in situ* color generation by mixing extrinsic structural color and intrinsic emission color on MAPbX₃ perovskite gratings.

are incident on the sample simultaneously. The fundamental pixel of the image is a one-dimensional (1D) perovskite grating with a finite number of periods and strip length. On one hand, the MAPbX₃ has refractive indices around 2.1–2.5 (see Supplementary Section 1) in the visible spectrum. This value is not high enough to generate bright-field structural colors with its own magnetic dipole and electric dipole resonances.^{20,43,44} But it is comparable to TiO₂ and thus can generate high reflection *via* a short-period array.^{21,45,46} On the other hand, as a direct band-gap semiconductor, MAPbBr₃ can emit PL (see Supplementary Section 1) or laser light and form emission

colors with intensities determined by the excitation. According to color mixing theory, a third color is able to be generated by mixing the other two colors, and the resulting hue can be easily tuned by varying their mixing ratio. Consequently, a promising dynamical color tuning scheme could be realized by mixing the extrinsic structural color with intrinsic emission color, where the former color acts as the base and the latter color functions as a photonic impurity. The resulting color can be dynamically and reversibly controlled through tuning the density of the pumping laser. Significantly, with the pumping-density-dependent color, our scheme could realize *in situ* color tuning by controlling the excitation. In addition, the color transition time is determined only by the buildup and ring-down time of the PL, which is on the order of nanoseconds^{35,47,48} and orders of magnitude faster than current technologies.^{25–28} Therefore, an *in situ*, dynamic, and reversible nanoprinting can be produced with MAPbX₃ gratings. The emission color can be extended to full color by varying the band-gap *via* the stoichiometry of halogen element.^{49,50}

Extrinsic Structural Colors. One-dimensional MAPbBr₃ gratings on a glass substrate are designed for structural colors, as schematically shown in Figure 1. The reflection spectra were numerically calculated under transverse magnetic field (TM, *E*-field perpendicular to the strip) polarized as the dashed lines shown in the left panel of Figure 2A. A sharp resonance along with a low flat background can be clearly observed. As the period (*p*) varies from 405 to 280 nm and the gap (*d*) varies from 70 to 163 nm, the reflection peak blue-shifts from 672 to 458 nm, while the peak value and the fwhm are preserved above 85% and below 20 nm, respectively. Thus, distinct colors from red to purple can be generated (see right panel in Figure 2A). To further investigate the color range, we have numerically calculated the structural colors generated from 1023 samples by varying the structural parameters *p* and *d* with a step of 5 nm. As shown in Figure 2B, a vivid color rainbow is presented, demonstrating the capability of perovskite gratings in distinct structural colors. We also find that the transverse electric (TE, *E* parallel to the strip) polarized reflection peak can also be formed (see Supplementary Section 2), but it is strongly affected by the quality of the film and the color impressions are usually worse. Below, we focus on the TM-polarized resonances.

The MAPbBr₃ gratings are fabricated with a top-down process (see Supplementary Section 1).⁵¹ The recorded reflection spectra are plotted as solid lines in Figure 2A. A series of intense reflection peaks can be seen, which match well the numerical results. The corresponding field patterns (see insets in Figure 2A) show that the reflection peaks are caused by the magnetic resonance and the collective effect.^{21,46} With the variation of structural parameters *p* and *d* (see SEM images in Figure 2A), the reflection peaks also linearly shift from 672 to 458 nm, covering most of the visible spectrum. Then the samples are placed under the bright field of the optical microscope (ZEISS, Axio Scope A1). The structural color varies from dark red to purple, which also matches the calculated color well, as shown in the right panel of Figure 2A.

The distinct colors are mainly attributed to the narrow and intensive reflection peaks. Due to the ion implanting in the top-down nanofabrication process, the band-edge of MAPbBr₃ is pushed to ~460 nm (see Supplementary Section 3).⁴¹ In this regard, the perovskite gratings are almost lossless in a spectral range above 460 nm and can produce high-reflection colors. Although etched nanostructures have extra scattering losses, the reflections are still ~40–65% with a fwhm ranging from

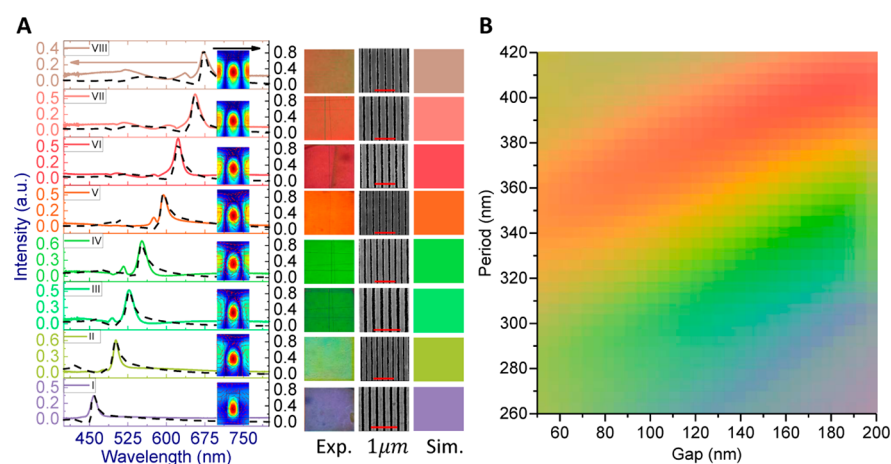


Figure 2. Extrinsic structural color by varying the periodicity of 1D MAPbBr₃ gratings. (A) Left panel shows the comparison of experimental reflection spectra (solid lines) and simulated counterparts (dash lines) as the period (p) and gap (d) vary, while the right panel shows the corresponding measured colors, SEM images, and calculated colors. Here the period in panels I–VIII is $p = 280, 280, 310, 320, 340, 382, 400,$ and 400 nm, and the gap in panels I–VIII is $d = 163, 107, 140, 105, 80, 110, 100,$ and 70 nm, respectively. The thicknesses of MAPbBr₃ films are 205 nm. All the scale bars are $1 \mu\text{m}$. (B) Numerical color palette obtained by stepwise tuning of p and d . The insets in (A) are their corresponding field patterns ($|H|$). The arrows correspond to the directions of electric currents.

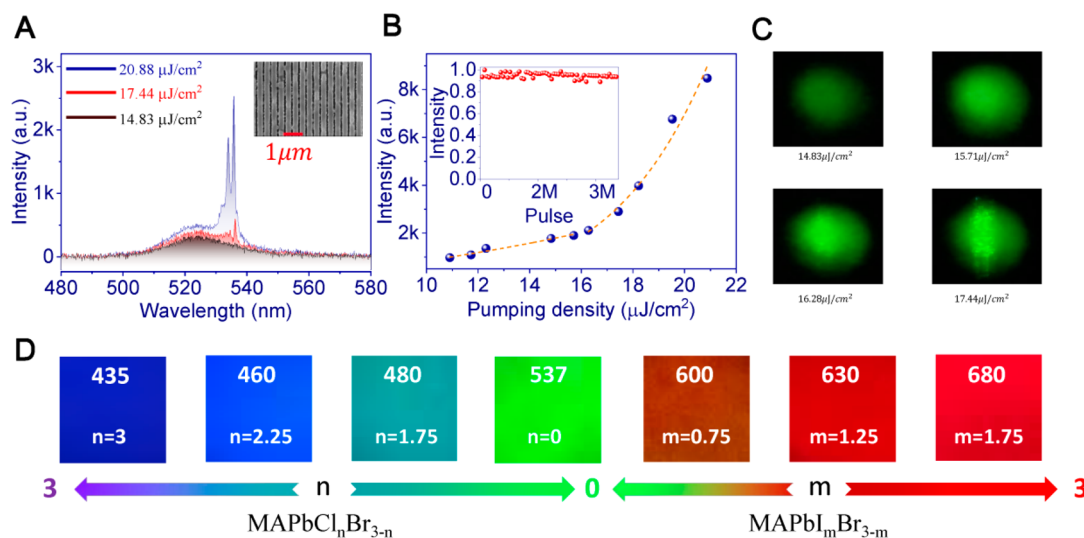


Figure 3. Intrinsic emission color generated by photoemission. (A) Emission spectra of MAPbBr₃ gratings with different pumping densities. The inset shows the top-view SEM image of the MAPbBr₃ gratings. (B) Output intensity as a function of pumping density. The inset shows the photostability of the MAPbBr₃ gratings under photon doping. (C) Fluorescent microscope images of MAPbBr₃ gratings with the increase of pumping density. (D) Vivid emission colors from blue to red of MAPbCl _{n} Br _{$3-n$} and MAPbI _{m} Br _{$3-m$} as stoichiometry varies. The corresponding stoichiometry is also listed.

13 to 20 nm (see Supplementary Section 3), which are superior to counterparts of MAPbI₃ gratings.⁵² In terms of quality factor ($Q = \lambda/\Delta\lambda$, here λ is the central wavelength and $\Delta\lambda$ is the fwhm), the Q values of reflection peaks are around 28–39, which is more than an order of magnitude larger than the counterpart on MAPbI₃ gratings.⁵²

Interestingly, the distinct structural colors also benefit from the material absorption. Apart from the main reflection peak, arising from low order diffraction, the grating also supports higher order reflection peaks within the visible range and thus spoils the color impressions (see Supplementary Section 4). For the designed MAPbBr₃ gratings, their higher order modes at shorter wavelengths are almost fully absorbed. Thus, the background is suppressed to improve the color impression. The effects of material absorption can be clearly seen in panel I

of Figure 2A. Once the reflection peak approaches the band-edge, the reflectance is drastically reduced to $\sim 30\%$.

Intrinsic Emission Colors from Photoemission. Besides the extrinsic structural colors, MAPbX₃ gratings also have intrinsic emissions originating from their direct band-gap. Taking the sample with $p = 325$ nm and $d = 100$ nm as an example, we have explored their emission properties *via* optical excitation (see Supplementary Section 5). As shown in Figure 3A, when the pumping density is $14.83 \mu\text{J}/\text{cm}^2$, a broad PL emission peak is centered at 524 nm with a fwhm of ~ 20 nm. As the pumping density increases to $17.44 \mu\text{J}/\text{cm}^2$, sharp peaks emerged and quickly dominated the emission spectrum, while the fwhm was significantly reduced to 0.7 nm, which was about 30 times smaller than the PL. Figure 3B shows the output intensity as a function of pumping density. The drastic increase in the power slope, associated with the sharp peaks and narrow

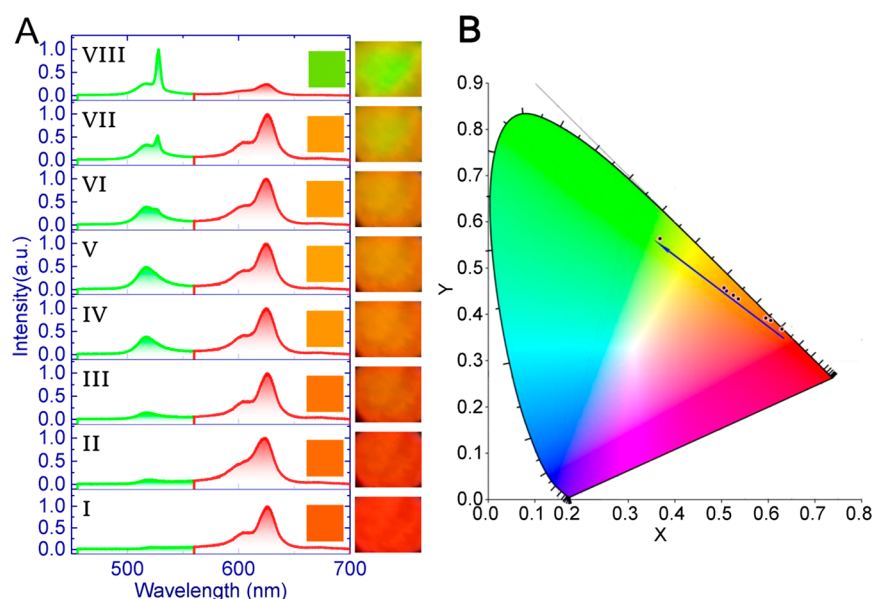


Figure 4. Dynamic control of color displays. (A) Recorded spectra and the corresponding colors of MAPbBr₃ gratings (period $p = 350$ nm, gap $d = 100$ nm, and thickness $h = 205$ nm) as a function of pumping density. The inset in each panel is the color calculated by relevant spectra; the left panel is experimentally recorded fluorescent microscope images. (B) Evolution of structural colors in the CIE 1931 color map.

fwhm, has confirmed the onset of perovskite gratings lasing. Figure 3C shows the experimentally recorded fluorescent microscope images. Even though the pumping power is very low, vivid green colors can still be seen. With the increase in pumping density, the brightness of the green color increases quickly. Finally, a bright laser spot emerges in the image and the intensity is dramatically increased (see Figure 3B). The emission color of perovskite gratings is found to be quite stable. As the inset shows in Figure 3B (see Supplementary Section 6), the total intensity decreases less than 10% when the MAPbBr₃ gratings is pumped with 3.6×10^6 laser shots. In addition, the emission color of MAPbBr₃ is not restricted to a green color. By thermal annealing the MAPbBr₃ in a low-pressure chemical vapor deposition with a CH₃NH₃I or CH₃NH₃Cl vapor environment, the bromide ions are substituted with chlorine ions or iodine ions. As a result, vibrant emission colors can spread from purple to red (see Figure 3D).

Reversible Interplay of the Extrinsic and Intrinsic Color. Based on the above observations, one MAPbX₃ gratings can support two types of colors, *i.e.*, extrinsic structural color and intrinsic emission color. Then, a mixed color can be obtained when a MAPbX₃ grating is illuminated by white light and laser light simultaneously. What is more, by controlling the brightness of the green colors with the laser pumping density (Figure 3C), the ratio of emission to reflection can be dynamically controlled. Therefore, although both colors are static, their mixture makes perovskite gratings ideal for the realization of dynamic color (see the schematic picture in Figure 1). To experimentally demonstrate this possibility, we have fabricated MAPbBr₃ gratings and studied their display color as a function of pumping density, as shown in Figure 4A. When the nanostructure was illuminated with only a white light source, a reflection peak occurred at ~ 625 nm and a bright red color could be observed. When the perovskite grating was photon doped by a Ti:sapphire laser (see Supplementary Section 6) simultaneously, an additional peak appeared at 515 nm. As the pumping power increased, the emission from perovskite got stronger

and became comparable to the reflection of white light. Correspondingly, the display color image also transitioned from red to orange and finally to chartreuse (see panels II–VII in Figure 4A). Furthermore, the emission intensity could surpass the reflection peak as the pumping intensity increases. As a result, a green color would be observed (see panel VIII in Figure 4A). The corresponding color coordinates were then calculated using the spectra in Figure 4A and plotted in the well-known CIE 1931 color map (see Figure 4B). While the structures, refractive indices, and stoichiometry of MAPbX₃ gratings are all fixed, the display color simply traverses different color regions by increasing external excitation. Significantly, with the decrease in pumping density, the reflection peak can be gradually recovered to its original position, and thus the dynamic color display is also reversible. Taking into account the nanosecond level transition time of emission color (see Supplementary Section 7), the color variation can respond on the same level, orders of magnitude faster than previous works.^{23–26} Due to a pumping-dependent color mixing mechanism, naturally, our design supports an *in situ* color control capability by moving the laser spot.

Now we show that an active grating has been applied to generate dynamically controlled color nanoprints in an *in situ* and reversible way. Besides, in combination with other emission colors (from blue to red) by varying the stoichiometry of MAPbX₃ gratings (see Figure 3D), the final colors could dynamically convert over a much larger range (see Supplementary Section 8 and Section 9).

In experiment, we found that a distinct structural color could be generated with only 7 periods (see Supplementary Section 10), supporting a color pixel with a lateral width as small as ~ 2.8 μm . Here, the length of each stripe is fixed at 3.5 μm . Thus, the spatial resolution can be larger than 7257 dot per inch (dpi), which is fine enough for most high spatial resolution display applications. To verify the capability of rendering a distinct color image, a sample was fabricated to demonstrate the logo of Harbin Institute of Technology with a size of 530 \times 610 μm^2 .

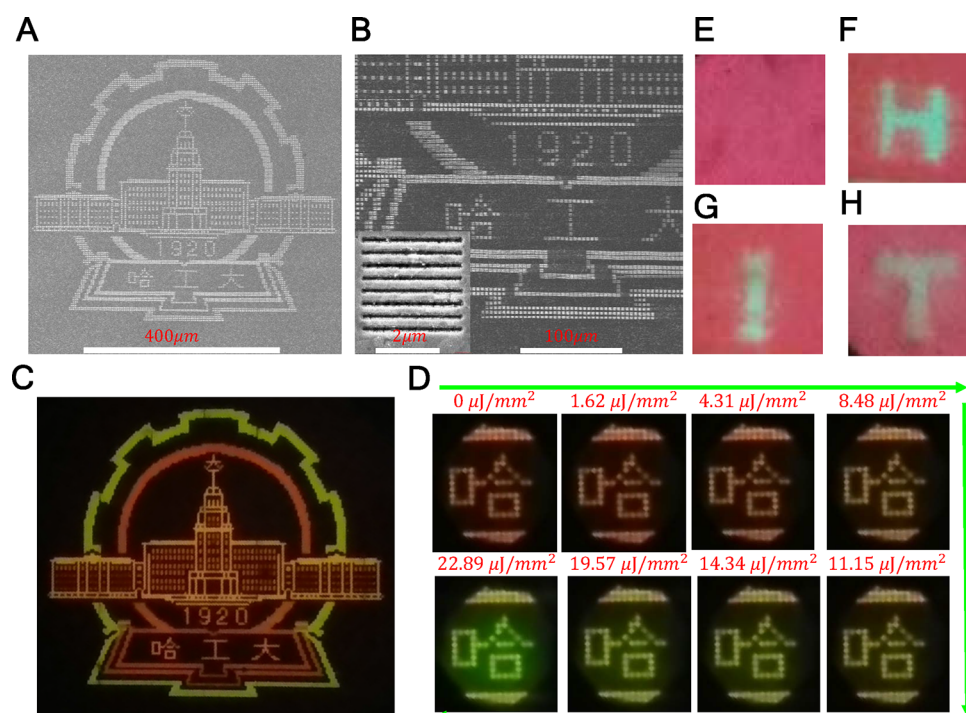


Figure 5. Dynamic color image printing with MAPbBr₃ gratings. (Logo printed with permission from Harbin Institute of Technology. Copyright 2018 Harbin Institute of Technology.) (A) Top-view SEM image of the logo of Harbin Institute of Technology. (B) Enlarged SEM image of partial university logo. The inset shows the high-resolution SEM image of one pixel of the logo. (C) Microscope image of the university logo without photon doping. (D) Microscope images of part of the university logo at different pumping densities. Here the pumping density increases along the green arrow from 0 to 22.89 $\mu\text{J}/\text{cm}^2$. (Logo printed with permission from Harbin Institute of Technology. Copyright 2016 Harbin Institute of Technology.) (E) Structural colors of the MAPbBr₃ meta-gratings. (G, H) Created images of the MAPbBr₃ meta-gratings with spatially modulated optical excitation.

Figure 5A and B show the top-view and partially zoomed-in SEM images of the fabricated structure, respectively. Based on the results in Figure 2, the colors at different locations have been predefined with different geometric parameters. Consequently, when the sample was illuminated by a white light source, a colorful image was successfully recorded by the CCD camera (see Figure 5C). In contrast to the conventional gratings, the colors in the university logo can also be dynamically controlled *via* external excitation. The color of the Chinese character 哈 has been successfully tuned from red to green (see Figure 5D) as the pumping density increased gradually. Therefore, we can confirm that the MAPbX₃ gratings can be used to generate distinct and dynamic display colors.

In addition to dynamic control of the structural colors in Figure 4, this technique also has the ability to create an image within a homogeneous color obtained with the white lamp. In this experiment, the pumping laser beam is spatially modulated to different shapes. After it is focused onto the MAPbBr₃ meta-gratings, the shapes of laser beam are well constructed and partially excite the nanostructure. As a result, the colors of the excited regions change and the modulated images are reproduced in the homogeneous color. One example is shown in the inset of Figure 5E–H. With the spatially modulated optical excitation, the characters “H”, “I”, and “T” have been created within the initial homogeneous color.

In both types of dynamic control of structural color, we note that the spatial resolution is determined by the large value between the sizes of gratings and the spatially modulated laser beam. According to the recent research, the pixel size of the spatially modulated laser beam is $\sim 1 \mu\text{m}$,⁵³ which is much smaller than the size of each meta-grating ($3.5 \mu\text{m} \times 3.5 \mu\text{m}$).

Therefore, the spatial resolution is still around 7257 dpi. Similar to the polarization dependence, this value can also be improved by using two-dimensional nanostructure based metasurfaces. We also note that the perovskite gratings in current research have several limitations such as polarization dependence and angular dependence (see Supplementary Section 12). Considering the angular independence of photoluminescence (see Supplementary Section 12), the latter can cause a color change at different angles of observation and hinder the possible applications. Fortunately, these limitations can be simply solved by utilizing the two-dimensional nanostructures (see Supplementary Section 12).^{21,54}

CONCLUSION

In summary, we have experimentally demonstrated an *in situ* dynamic color display by photonically doping MAPbX₃ gratings, which was enabled by the interplay of extrinsic structural color and intrinsic emission color. The presented color could be tuned over a large color gamut by modifying the emission intensity, which is dependent on the external pumping light density and can be simply controlled. The color gamut can be further enlarged by varying the stoichiometry of MAPbX₃. Compared with previous reports, our MAPbX₃-based approach has a series of advantages in color generation, especially the capability of *in situ* control and a nonvacuum environment. Importantly, our design principle can be readily extended to other gain materials such as GaN, ZnO, and CdS. We believe that our design presents a promising realization of *in situ* dynamic color nanoprinting and will empower important advances in structural color, classified nanoprinting, augmented reality devices, and biosensing.

METHODS

Fabrication of the Perovskite Thin Films. The MAPbX₃ thin films were synthesized with the solution-based one-step method.^{55–57} First, 3 mmol of CH₃NH₃Br (99%, Materwin) and 3 mmol of PbBr₂ (99%, Materwin) were dissolved in 2 mL of dimethyl sulfoxide (DMSO, Aladin-e, D103279-500 mL) individually and form the CH₃NH₃Br-PbBr₂ stock solution (with a concentration of 1.5 mmol/mL). Then 50 μ L of stock solution was dropped and spin-coated on the substrate at 5000 rpm for 60 s with an 800 L/h nitrogen gas blowing over the film. After 24 s of spin-coating, 30 μ L of chlorobenzene (AR, Dmreagent) was added to the film to accelerate the nucleation, precipitation, and crystallization in the film.

Fabrication of MAPbBr₃ Gratings. The fabrication process of MAPbBr₃ gratings includes an electron-beam lithography (EBL, Raith E-line) and an inductively coupled plasma etching (ICP, Oxford, System100 ICP180). During the first process, a 300 nm electron-beam resist (ZEP 520A) was spin-coated onto the perovskite film and then patterned by an electron beam writer with a dose 56 μ C/cm² under an acceleration voltage of 30 kV. After developing in N50, the pattern of gratings was generated within the resist. Then the sample was etched with an Oxford Instruments Plasma Technology 380 plasma source. The chamber was pumped to reach a degree of vacuum around 10⁻⁹ Torr. Then the MAPbBr₃ film was etched by chlorine gas with a 5 sccm flow rate. During the etching, C₄F₈ with a 10 sccm flow rate was used as a protective gas. The ICP power was 600 W, and the RF power was 150 W.

Control of Stoichiometry of Perovskite. The chemical doping of the perovskite nanostructure was done using chemical vapor deposition (CVD, home-built with OTF-1200X, GSL-32, GZK 101, from MTI Corporation). During the whole vapor conversion process, the CH₃NH₃I (99%, Materwin) or CH₃NH₃Br (99%, Materwin) powder was placed at the center of a CVD furnace while the perovskite nanostructure (placed on a substrate) was mounted downstream of the apparatus. Ar and H₂ were used as carrier gases with flow rates of 25 and 15 sccm, respectively. The central heating zone was increased to 130 °C (CH₃NH₃I) or 120 °C (CH₃NH₃Cl) (8 °C/min heating rate, 10 min as buffer) under low-pressure conditions (40–50 Torr) and maintained for a few hours (the speed of the moving emitted peak is about 10 nm/30 min). The furnace was then naturally cooled to room temperature.

Numerical Calculation. The numerical calculations were performed with a commercial finite element method software (Comsol Multiphysics 4.3a). During the simulation, one unit cell with periodic boundary conditions has been used. The material dispersion and the refractive index of the substrate are both considered (see Supplementary Section 1).

Optical Measurement. The nanostructures are placed onto a three-dimensional translation stage under an optical microscope (ZEISS, Axio Scope A1). A white light (Thorlabs, SLS201/M) and a frequency-doubled Ti:sapphire laser (Spectra-Physics, 400 nm, 1k Hz repetition rate, 100 fs pulse duration) are focused by an objective lens (20 \times with NA = 0.4) onto the top surface of the samples. The reflected light and the photoluminescence of perovskite nanostructures are collected by the same objective lens and coupled to a spectrometer (Princeton Instruments, SCT320 with Pixis 256). The bright-field images are recorded by a camera (Canon EOS 600D).

ASSOCIATED CONTENT

Supporting Information

The Supporting Information is available free of charge on the ACS Publications website at DOI: 10.1021/acsnano.8b02425.

Additional information (PDF)

AUTHOR INFORMATION

Corresponding Authors

*E-mail: chengwei.qiu@nus.edu.sg.

*E-mail: qinghai.song@hit.edu.cn.

*E-mail: shumini.xiao@hit.edu.cn.

ORCID

Qinghai Song: 0000-0003-1048-411X

Shumin Xiao: 0000-0002-0751-9556

Author Contributions

*Y. Gao and C. Huang contributed equally.

Notes

The authors declare no competing financial interest.

ACKNOWLEDGMENTS

This research is finally supported by Shenzhen Fundamental Research Projects (Grant No. JCYJ20160505175637639), Public Platform for Fabrication and Detection of Micro- & Nanosized Aerospace Devices, and Shenzhen Engineering Laboratory on Organic–Inorganic Perovskite Devices. C.W.Q. acknowledges financial support from the A*STAR Pharos Program (Grant No. 1527000014, with Project No. R-263-000-B91-305) and the National Research Foundation, Prime Minister's Office, under its Competitive Research Programme (CRP Award No. NRF-CRP15-2015-03).

REFERENCES

- (1) Sato, O.; Kubo, S.; Gu, Z. Structural Color Films with Lotus Effects, Superhydrophilicity, and Tunable Stop-bands. *Acc. Chem. Res.* **2008**, *42*, 1–10.
- (2) Zi, J.; Yu, X.; Li, Y.; Hu, X.; Xu, C.; Wang, X.; Liu, X.; Fu, R. Coloration Strategies in Peacock Feathers. *Proc. Natl. Acad. Sci. U. S. A.* **2003**, *100*, 12576–12578.
- (3) Noh, H.; Liew, S. F.; Saranathan, V.; Mochrie, S. G.; Prum, R. O.; Dufresne, E. R.; Cao, H. How Noniridescent Colors Are Generated by Quasi-ordered Structures of Bird Feathers. *Adv. Mater.* **2010**, *22*, 2871–2880.
- (4) Parker, A. R.; Welch, V. L.; Driver, D.; Martini, N. Structural Colour: Opal Analogue Discovered in a Weevil. *Nature* **2003**, *426*, 786–787.
- (5) Vukusic, P.; Sambles, J. R. Photonic Structures in Biology. *Nature* **2003**, *424*, 852–855.
- (6) Vignolini, S.; Rudall, P. J.; Rowland, A. V.; Reed, A.; Moyroud, E.; Faden, R. B.; Baumberg, J. J.; Glover, B. J.; Steiner, U. Pointillist Structural Color in Pollia Fruit. *Proc. Natl. Acad. Sci. U. S. A.* **2012**, *109*, 15712–15715.
- (7) Prum, R. O.; Torres, R. H.; Williamson, A. S.; Dyck, J. Coherent Light Scattering by Blue Feather Barbs. *Nature* **1998**, *396*, 28–29.
- (8) Chung, K.; Yu, S.; Heo, C. J.; Shim, J. W.; Yang, S. M.; Han, M. G.; Lee, H. S.; Jin, Y.; Lee, S. Y.; Park, N. Flexible, Angle-Independent, Structural Color Reflectors Inspired by Morpho Butterfly Wings. *Adv. Mater.* **2012**, *24*, 2375–2379.
- (9) Forster, J. D.; Noh, H.; Liew, S. F.; Saranathan, V.; Schreck, C. F.; Yang, L.; Park, J. G.; Prum, R. O.; Mochrie, S. G.; O'Hern, C. S. Biomimetic Isotropic Nanostructures for Structural Coloration. *Adv. Mater.* **2010**, *22*, 2939–2944.
- (10) Kats, M. A.; Capasso, F. Optical Absorbers Based on Strong Interference in Ultra-thin Films. *Laser Photonics Rev.* **2016**, *10*, 735–749.
- (11) Kristensen, A.; Yang, J. K. W.; Bozhevolnyi, S. I.; Link, S.; Nordlander, P.; Halas, N. J.; Mortensen, N. A. Plasmonic Colour Generation. *Nat. Rev. Mater.* **2017**, *2*, 16088.
- (12) Kumar, K.; Duan, H.; Hegde, R. S.; Koh, S. C.; Wei, J. N.; Yang, J. K. Printing Colour at the Optical Diffraction Limit. *Nat. Nanotechnol.* **2012**, *7*, 557–561.
- (13) Xiong, K.; Emilsson, G.; Maziz, A.; Yang, X.; Shao, L.; Jager, E. W.; Dahlin, A. B. Plasmonic Metasurfaces with Conjugated Polymers for Flexible Electronic Paper in Color. *Adv. Mater.* **2016**, *28*, 9956–9960.

- (14) Miyata, M.; Hatada, H.; Takahara, J. Full-color Subwavelength Printing with Gap-plasmonic Optical Antennas. *Nano Lett.* **2016**, *16*, 3166–3172.
- (15) Gu, Y.; Zhang, L.; Yang, J. K.; Yeo, S. P.; Qiu, C.-W. Color Generation via Subwavelength Plasmonic Nanostructures. *Nanoscale* **2015**, *7*, 6409–6419.
- (16) Lee, K.-T.; Jang, J.-Y.; Park, S. J.; Thakur, U. K.; Ji, C.; Guo, L. J.; Park, H. J. Subwavelength Nanocavity for Flexible Structural Transmissive Color Generation with a Wide Viewing Angle. *Optica* **2016**, *3*, 1489–1495.
- (17) Olson, J.; Manjavacas, A.; Liu, L.; Chang, W.-S.; Foerster, B.; King, N. S.; Knight, M. W.; Nordlander, P.; Halas, N. J.; Link, S. Vivid, Full-color Aluminum Plasmonic Pixels. *Proc. Natl. Acad. Sci. U. S. A.* **2014**, *111*, 14348–14353.
- (18) Kats, M. A.; Blanchard, R.; Genevet, P.; Capasso, F. Nanometre Optical Coatings Based on Strong Interference Effects in Highly Absorbing Media. *Nat. Mater.* **2013**, *12*, 20.
- (19) Naik, G. V.; Shalae, V. M.; Boltasseva, A. Alternative Plasmonic Materials: beyond Gold and Silver. *Adv. Mater.* **2013**, *25*, 3264–3294.
- (20) Proust, J.; Bedu, F. d. r.; Gallas, B.; Ozerov, I.; Bonod, N. All-dielectric Colored Metasurfaces with Silicon Mie Resonators. *ACS Nano* **2016**, *10*, 7761–7767.
- (21) Sun, S.; Zhou, Z.; Zhang, C.; Gao, Y.; Duan, Z.; Xiao, S.; Song, Q. All-dielectric Full-color Printing with TiO₂ Metasurfaces. *ACS Nano* **2017**, *11*, 4445–4452.
- (22) Cao, L.; Fan, P.; Barnard, E. S.; Brown, A. M.; Brongersma, M. L. Tuning the Color of Silicon Nanostructures. *Nano Lett.* **2010**, *10*, 2649–2654.
- (23) Kuznetsov, A. I.; Miroshnichenko, A. E.; Brongersma, M. L.; Kivshar, Y. S.; Luk'yanchuk, B. Optically Resonant Dielectric Nanostructures. *Science* **2016**, *354*, aag2472.
- (24) Nagasaki, Y.; Suzuki, M.; Takahara, J. All-Dielectric Dual-Color Pixel with Subwavelength Resolution. *Nano Lett.* **2017**, *17*, 7500–7506.
- (25) Franklin, D.; Chen, Y.; Vazquez-Guardado, A.; Modak, S.; Boroumand, J.; Xu, D.; Wu, S.-T.; Chanda, D. Polarization-independent Actively Tunable Colour Generation on Imprinted Plasmonic Surfaces. *Nat. Commun.* **2015**, *6*, 7337.
- (26) Liu, Y. J.; Si, G. Y.; Leong, E. S.; Xiang, N.; Danner, A. J.; Teng, J. H. Light-driven Plasmonic Color Filters by Overlaying Photo-responsive Liquid Crystals on Gold Annular Aperture Arrays. *Adv. Mater.* **2012**, *24*, OP131–OP135.
- (27) Duan, X.; Kamin, S.; Liu, N. Dynamic Plasmonic Colour Display. *Nat. Commun.* **2017**, *8*, 14606.
- (28) Chen, Y.; Duan, X.; Matuschek, M.; Zhou, Y.; Neubrech, F.; Duan, H.; Liu, N. Dynamic Color Displays Using Stepwise Cavity Resonators. *Nano Lett.* **2017**, *17*, 5555–5560.
- (29) Tseng, M. L.; Yang, J.; Semmlinger, M.; Zhang, C.; Nordlander, P.; Halas, N. J. Two-Dimensional Active Tuning of an Aluminum Plasmonic Array for Full-Spectrum Response. *Nano Lett.* **2017**, *17*, 6034–6039.
- (30) Stec, G. J.; Lauchner, A.; Cui, Y.; Nordlander, P.; Halas, N. J. Multicolor Electrochromic Devices Based on Molecular Plasmonics. *ACS Nano* **2017**, *11*, 3254–3261.
- (31) Olson, J.; Manjavacas, A.; Basu, T.; Huang, D.; Schlather, A. E.; Zheng, B.; Halas, N. J.; Nordlander, P.; Link, S. High Chromaticity Aluminum Plasmonic Pixels for Active Liquid Crystal Displays. *ACS Nano* **2016**, *10*, 1108–1117.
- (32) Stranks, S. D.; Snaith, H. J. Metal-halide Perovskites for Photovoltaic and Light-emitting Devices. *Nat. Nanotechnol.* **2015**, *10*, 391–402.
- (33) Sutherland, B. R.; Sargent, E. H. Perovskite Photonic Sources. *Nat. Photonics* **2016**, *10*, 295–302.
- (34) Eaton, S. W.; Lai, M.; Gibson, N. A.; Wong, A. B.; Dou, L.; Ma, J.; Wang, L.-W.; Leone, S. R.; Yang, P. Lasing in Robust Cesium Lead Halide Perovskite Nanowires. *Proc. Natl. Acad. Sci. U. S. A.* **2016**, *113*, 1993–1998.
- (35) Xing, G.; Mathews, N.; Lim, S. S.; Yantara, N.; Liu, X.; Sabba, D.; Grätzel, M.; Mhaisalkar, S.; Sum, T. C. Low-temperature Solution-processed Wavelength-tunable Perovskites for Lasing. *Nat. Mater.* **2014**, *13*, 476.
- (36) Zhou, H.; Yuan, S.; Wang, X.; Xu, T.; Wang, X.; Li, H.; Zheng, W.; Fan, P.; Li, Y.; Sun, L.; Pan, A. Vapor Growth and Tunable Lasing of Band Gap Engineered Cesium Lead Halide Perovskite Micro/Nanorods with Triangular Cross Section. *ACS Nano* **2017**, *11*, 1189–1195.
- (37) Pan, A.; Yang, H.; Liu, R.; Yu, R.; Zou, B.; Wang, Z. Color-tunable Photoluminescence of Alloyed CdS_xSe_{1-x} Nanobelts. *J. Am. Chem. Soc.* **2005**, *127*, 15692–15693.
- (38) Zhang, Q.; Ha, S. T.; Liu, X.; Sum, T. C.; Xiong, Q. Room-temperature Near-infrared High-Q Perovskite Whispering-gallery Planar Nanolasers. *Nano Lett.* **2014**, *14*, 5995–6001.
- (39) Xing, J.; Yan, F.; Zhao, Y.; Chen, S.; Yu, H.; Zhang, Q.; Zeng, R.; Demir, H. V.; Sun, X.; Huan, A.; Xiong, Q. High-Efficiency Light-Emitting Diodes of Organometal Halide Perovskite Amorphous Nanoparticles. *ACS Nano* **2016**, *10*, 6623–6630.
- (40) Huang, H.; Raith, J.; Kershaw, S. V.; Kalytchuk, S.; Tomanec, O.; Jing, L.; Susha, A. S.; Zboril, R.; Rogach, A. L. Growth Mechanism of Strongly Emitting CH₃NH₃PbBr₃ Perovskite Nanocrystals with a Tunable Bandgap. *Nat. Commun.* **2017**, *8*, 996.
- (41) Zhang, N.; Wang, K.; Wei, H.; Gu, Z.; Sun, W.; Li, J.; Xiao, S.; Song, Q. Postsynthetic and Selective Control of Lead Halide Perovskite Microlasers. *J. Phys. Chem. Lett.* **2016**, *7*, 3886–3891.
- (42) Xiao, Z.; Kerner, R. A.; Zhao, L.; Tran, N. L.; Lee, K. M.; Koh, T.-W.; Scholes, G. D.; Rand, B. P. Efficient Perovskite Light-emitting Diodes Featuring Nanometre-sized Crystallites. *Nat. Photonics* **2017**, *11*, 108–115.
- (43) Tiguntseva, E. Y.; Zograf, G. P.; Komissarenko, F. E.; Zuev, D. A.; Zakhidov, A. A.; Makarov, S. V.; Kivshar, Y. S. Light-Emitting Halide Perovskite Nanoantennas. *Nano Lett.* **2018**, *18*, 1185–1190.
- (44) Makarov, S. V.; Milichko, V.; Ushakova, E. V.; Omelyanovich, M.; Cerdan Pasaran, A.; Haroldson, R.; Balachandran, B.; Wang, H.; Hu, W.; Kivshar, Y. S.; Zakhidov, A. A. Multifold Emission Enhancement in Nanoimprinted Hybrid Perovskite Metasurfaces. *ACS Photonics* **2017**, *4*, 728–735.
- (45) Sun, S.; Yang, W.; Zhang, C.; Jing, J.; Gao, Y.; Yu, X.; Song, Q.; Xiao, S. Real-Time Tunable Colors from Microfluidic Reconfigurable All-Dielectric Metasurfaces. *ACS Nano* **2018**, *12*, 2151–2159.
- (46) Shen, Y.; Rinnerbauer, V.; Wang, L.; Stelmakh, V.; Joannopoulos, J. D.; Soljačić, M. Structural Colors from Fano Resonances. *ACS Photonics* **2015**, *2*, 27–32.
- (47) Yi, N.; Wang, S.; Duan, Z.; Wang, K.; Song, Q.; Xiao, S. Tailoring the Performances of Lead Halide Perovskite Devices with Electron-Beam Irradiation. *Adv. Mater.* **2017**, *29*, 1701636.
- (48) Liao, Q.; Hu, K.; Zhang, H.; Wang, X.; Yao, J.; Fu, H. Perovskite Microdisk Microlasers Self-Assembled from Solution. *Adv. Mater.* **2015**, *27*, 3405–3410.
- (49) He, X.; Liu, P.; Wu, S.; Liao, Q.; Yao, J.; Fu, H. Multi-color Perovskite Nanowire Lasers through Kinetically Controlled Solution Growth Followed by Gas-phase Halide Exchange. *J. Mater. Chem. C* **2017**, *5*, 12707–12713.
- (50) Huang, H.; Polavarapu, L.; Sichert, J. A.; Susha, A. S.; Urban, A. S.; Rogach, A. L. Colloidal Lead Halide Perovskite Nanocrystals: Synthesis, Optical Properties and Applications. *NPG Asia Mater.* **2016**, *8*, e328.
- (51) Zhang, N.; Sun, W.; Rodrigues, S. P.; Wang, K.; Gu, Z.; Wang, S.; Cai, W.; Xiao, S.; Song, Q. Highly Reproducible Organometallic Halide Perovskite Microdevices Based on Top-Down Lithography. *Adv. Mater.* **2017**, *29*, 1606205.
- (52) Gholipour, B.; Adamo, G.; Cortecchia, D.; Krishnamoorthy, H. N.; Birowosuto, M. D.; Zheludev, N. I.; Soci, C. Organometallic Perovskite Metasurfaces. *Adv. Mater.* **2017**, *29*, 5.
- (53) Auyeung, R. C.; Kim, H.; Mathews, S.; Pique, A. Spatially modulated laser pulses for printing electronics. *Appl. Opt.* **2015**, *54*, F70–F77.

(54) Dong, Z.; Ho, J.; Yu, Y. F.; Fu, Y. H.; Paniagua-Dominguez, R.; Wang, S.; Kuznetsov, A. I.; Yang, J. K. W. Printing Beyond sRGB Color Gamut by Mimicking Silicon Nanostructures in Free-Space. *Nano Lett.* **2017**, *17*, 7620–7628.

(55) Xia, B.; Wu, Z.; Dong, H.; Xi, J.; Wu, W.; Lei, T.; Xi, K.; Yuan, F.; Jiao, B.; Xiao, L.; Gong, Q.; Hou, X. Formation of Ultrasmooth Perovskite Films Toward Highly Efficient Inverted Planar Heterojunction Solar Cells By Micro-flowing Anti-solvent Deposition in Air. *J. Mater. Chem. A* **2016**, *4*, 6295–6303.

(56) Long, M.; Zhang, T.; Chai, Y.; Ng, C. F.; Mak, T. C.; Xu, J.; Yan, K. Nonstoichiometric Acid-base Reaction as Reliable Synthetic Route to Highly Stable $\text{CH}_3\text{NH}_3\text{PbI}_3$ Perovskite Film. *Nat. Commun.* **2016**, *7*, 13503.

(57) Zhang, T.; Long, M.; Yan, K.; Zeng, X.; Zhou, F.; Chen, Z.; Wan, X.; Chen, K.; Liu, P.; Li, F.; Yu, T.; Xie, W.; Xu, J. Facet-Dependent Property of Sequentially Deposited Perovskite Thin Films: Chemical Origin and Self-Annihilation. *ACS Appl. Mater. Interfaces* **2016**, *8*, 32366–32375.